

## An experimental study on the ballistic performance of FRP-steel plates completely penetrated by a hemispherical-nosed projectile

Changhai Chen<sup>\*1</sup>, Xi Zhu<sup>1a</sup>, Hailiang Hou<sup>1</sup>,  
Lijun Zhang<sup>1</sup>, Xiaole Shen<sup>2</sup> and Ting Tang<sup>1</sup>

<sup>1</sup> Department of Naval Architecture Engineering, Naval University of Engineering, Wuhan 430033, PR China  
<sup>2</sup> Lvshun Proving Ground, Naval Unit No. 91439, Dalian 116041, PR China

(Received November 18, 2012, Revised October 20, 2013, Accepted October 30, 2013)

**Abstract.** Experiments were carried out to investigate the ballistic performance of fiber reinforced plastic (FRP)-steel plates completely penetrated by hemispherical-nosed projectiles at sub-ordnance velocities greater than their ballistic limits. The FRP-steel plate consists of a front FRP laminate and a steel backing plate. Failure mechanisms and impact energy absorptions of FRP-steel plates were analyzed and compared with FRP laminates and single steel plates. The effects of relative thickness, manufacturing method and fabric type of front composite armors as well as the joining style between front composite armors and steel backing plates on the total perforation resistance of FRP-steel plates were explored. It is found that in the case of FRP-steel plates completely penetrated by hemispherical-nosed projectiles at low velocities, the failure modes of front composite armors are slightly changed while for steel backing plates, the dominate failure modes are greatly changed due to the influence of front composite armors. The relative thickness and fabric type of front composite armors as well as the joining style of FRP-steel plates have large effects whereas the manufacturing method of front composite armors has slight effect on the total perforation resistance of FRP-steel plates.

**Keywords:** ballistic performance; perforation; composite armor; low-velocity impact; hemispherical-nosed projectile

### 1. Introduction

The ballistic performance of multi-layered structures against projectile impact has long been of practical interest and many investigations in this aspect had been carried out over the past several decades. Early in 1970s, Kreyenhagen *et al.* (1970) performed two-dimensional numerical analyses of projectile hypervelocity impacts into multi-material laminated targets and two failure modes were identified for the back aluminum layers. Marom and Bodner (1979) conducted a series of tests and found that in-contact multi-layered beams were more effective than monolithic beams of equivalent weight under projectile impact while spaced multi-layered beams had inferior

\*Corresponding author, Mr., E-mail: [chenchanghai0746@163.com](mailto:chenchanghai0746@163.com)

<sup>a</sup> Professor, E-mail: [zhuxi816@163.com](mailto:zhuxi816@163.com)

ballistic resistance. Corran *et al.* (1983) experimentally studied the ballistic performance of multi-layered metallic plates and showed that layers placed in contact were superior to equivalent monolithic plates. However, an opposite conclusion was obtained by Radin and Goldsmith (1988). They conducted an investigation of ballistic resistance of multi-layered plates normally impacted by hard-steel flat and conical-nosed projectiles. They found that adjacent targets were less effective than equivalent monolithic targets. Similar findings were obtained by Nurick and Walter (1990). Through extensive experiments, Almohandes *et al.* (1996) investigated the ballistic resistance of steel-fiberglass layered plates impacted by 7.62 mm standard bullets. Results showed that single targets are more effective than layered targets of the same total thickness. Gupta and Madhu (1997) studied the impact of armor-piercing projectiles on layered metallic plates of various thicknesses and found that for relatively thick plates in two layers, the ballistic resistance was comparable to single plates of the same thicknesses, whereas for thin plates in contact, layered targets were inferior. Ben-Dor *et al.* (1998a) studied high-velocity penetration of rigid sharp impactors into ductile layered targets with air gaps between layers. It was found that the ballistic performance of layered targets is independent of the air gap widths and on the sequence of the layers. While a parallel study by Ben-Dor *et al.* (1998b) showed that the ballistic limit velocity of the layered target increases with the increase of the widths of the air gaps. Further discussion was presented in a recent paper by Ben-Dor *et al.* (2006), where it was concluded that the effect of air gaps is insignificant as long as the projectile is non-conical.

Experimental study on the perforation of laminated aluminum alloy targets by flat-ended and conical-tipped projectiles was described by Woodward and Cimpoeru (1998). It was showed that double-layered targets having two layers of equal thickness provided relatively higher ballistic limits than single targets of equivalent total thickness for both nose shapes. However, on a basis of a numerical study, Zukas and Scheffler (2001) concluded that layering dramatically weakened thin and intermediately thick targets. Similar results were obtained by Elek *et al.* (2005). Recently, an analytical model was developed by Liang *et al.* (2005) to evaluate the ballistic-resistant performance of multilayered targets. They found that the ballistic performance of single targets is the best. Previous work on the perforation resistance of double-layered steel plates by Dey *et al.* (2007) showed that in the case of blunt projectiles a large gain in the ballistic limit was obtained by layering the target and the overall protection level increased regardless of the projectile nose shapes. These findings were confirmed by Teng *et al.* (2007, 2008). Nevertheless, different results were obtained by Gupta *et al.* (2008), in which their investigation showed that for double-layered targets, the ballistic resistances were comparable to those for single plates of equivalent thicknesses, while an experimental study by Nia and Hoseini (2011) of the perforation of single and triple-layered Al targets by hemispherical-nosed projectiles showed that single targets have greater ballistic limits.

Although other similar studies can be found in the open literatures, results of the literatures reviewed above on the ballistic resistance of multi-layered targets are different even sometimes contradictory from each other so it is difficult to make comparisons between them due to the complexity of the impact process. Nevertheless, the search for improving ballistic performance of armors within restrictive weight requirement led inevitably the favor to high performance nonmetallic materials rather than metals. Zhu *et al.* (2003) experimentally investigated the ballistic resistance of warship light composite armor and found that light composite armors were much more effective than single steel plates within weight requirement. Meanwhile, they noticed that the ballistic resistance of combined targets increased with increasing the space between layers. These findings were also obtained by Zhu *et al.* (2006). Similar study on the ballistic performance of

combined targets, which consisted of a front composite armor and a steel backing plate, was conducted by Chen *et al.* (2011). Results showed that the ballistic resistance of combined targets was largely higher than that of single steel plates.

However, currently, few experimental researches into the ballistic resistance of FRP-steel plates were conducted. In present article, experiments were carried out to study the ballistic performance of FRP-steel plates to simulate warship topside composite armor systems which consists of a front FRP laminate and a steel backing plate, completely penetrated by hemispherical-nosed projectiles at velocities ranging from 200 to 400 m s<sup>-1</sup>. The background of this research is that the current warship topside composite armor system, which was commonly combined with composite laminates at the front and shipboard steel plates at the back, was completely penetrated by a semi-armor-piercing missile warhead, whose initial impact velocity was in the sub-ordnance velocity range with the velocity range 200 to 400 m s<sup>-1</sup> being the most common for current semi-armor-piercing missiles. For the purpose of comparison, single steel plates and FRP laminates were tested. All targets were normally perforated by hemispherical-nosed projectiles in sub-ordnance velocity range above their ballistic limits. Failure mechanisms and impact energy absorptions of FRP-steel plates were analyzed and compared with FRP laminates and single steel plates. The effects of joining style of FRP-steel plates and the relative thickness, manufacturing method and fabric type of front composite armors on the total perforation resistance of the FRP-steel plates were explored.

## 2. Experimental procedure

### 2.1 Targets

All tested targets had square dimensions 350 mm by 350 mm. Three types of targets were employed, namely single steel plates, FRP laminates and FRP-steel plates. A FRP-steel plate consists of a front FRP laminate (hereinafter called front composite armor) backed by a steel plate (hereinafter called steel backing plate). Steel backing plates are of the same materials as those for single steel plates and all of them were made of Q235 mild steel, which is an as received commercially structural steel. The main material properties of Q235 mild steel were obtained through quasi-static uniaxial tests as listed in Table 1.

FRP laminates were made of CT736 plain-woven fabrics through hot molding by a compression molding press. However, for front composite armors in FRP-steel plates, three types of plain-woven fabrics, i.e., CT736, T750 and SW220, were employed and two manufacturing methods (i.e. hot molding and hand lay-up) were adopted. The specifications of CT736, T750 and SW220 plain-woven fabrics were tabulated in Table 2. For FRP-steel plates (targets 1-8 except target 9), steel backing plate was adhesively bonded using epoxy resin on the rear side of front composite armor. The target specifications and their configurations were shown in Table 3.

Table 1 Material parameters of Q235 mild steel

Mass density $\rho_s / (\text{kg/m}^3)$	Young's modulus $E / \text{GPa}$	Poisson's Ratio $\nu$	Strain hardening modulus $E_h / \text{MPa}$	Yield strength $\sigma_y / \text{MPa}$	Ultimate tensile Strength $\sigma_u / \text{MPa}$	Elongation $\delta_s / \%$
7800	210	0.30	250	235	400-490	35

Table 2 Specifications of different fabrics and PC sheet

No.	Fabric type	Areal density /(g/cm <sup>2</sup> )	Thickness per ply /mm	Tension strength at break (Warp/Weft)	Construction
1	PC sheet	150	0.125	312.5 N/5cm or 50 MPa	—
2	CT736	410	0.60	15800/16400 N/5cm or 526.7/526.7 MPa	Plain-woven
3	T750	460	0.65	14000/14000 N/5cm or 430.8/430.8 MPa	Plain-woven
4	SW220	230	0.22	4000/3500 N/5cm or 363.6/318.2 MPa	Plain-woven

Table 3 Targets specifications and their configurations

Target number	Fabric type	Number of fabric plies	Manufacturing method	Joining style	Target type
1	—	—	—	—	Steel plates
2	CT736	6	Hot molding	—	FRP laminates
3	CT736	6	Hot molding	Adhesive bonding	FRP-steel plates
4	CT736	3	Hot molding	Adhesive bonding	FRP-steel plates
5	CT736	9	Hot molding	Adhesive bonding	FRP-steel plates
6	CT736	6	Hand lay-up	Adhesive bonding	FRP-steel plates
7	SW220	12	Hot molding	Adhesive bonding	FRP-steel plates
8	T750	6	Hot molding	Adhesive bonding	FRP-steel plates
9	T750	6	Hot molding	In-contact	FRP-steel plates

Table 4 Material properties of FRP laminates and front composite armors

Type of FRP	CT736/PC	CT736/epoxy	T750/PC	SW220/PC
Mass density $\rho_c$ /(kg/m <sup>3</sup> )	1650	1650	1600	2100
Elastic modulus $E$ /GPa	23.6	23.5	23.0	30.5
Compressive strength $\sigma_c$ /MPa	580.6	582.1	570.5	488.3
Ultimate tensile strength $\sigma_t$ /MPa	489	485	426	450
Shear modulus $E_S$ /GPa	0.68	0.70	0.67	1.11
Shear strength $\tau_s$ /MPa	180	185	174	156
Fracture toughness $G_c$ /(J/cm <sup>2</sup> )	2.42	2.39	1.88	1.59
Elongation $\delta$ /%	2.1	2.1	1.9	1.5
Specific strain energy absorption /(MJ/m <sup>3</sup> )	4.67	4.65	4.05	3.38

The hot-molding process mainly included the tailoring of fabric, the drying of fabric in a constant temperature box and hot molding by a compression molding press. The molded laminates were processed by compressing layers of fabric and polycarbonate sheet (PC sheet as shown in Table 2) stacking between the hot platens of the compression molding press. The platens were electrically heated to 210°C and at 3 MPa applied on the material. After an hour, the sample was

cooled under room temperature condition. For front composite armors manufactured using hand lay-up method, fabrics were flattened and then bonded evenly using a scraper by the glue after tailoring and drying of the fabrics. The glue was prepared in the laboratory by mixing 10 parts of epoxy resin adhesive with 10 parts of hardener. The glued fabrics, whilst still wet, were then pressed using weights and dried under room temperature condition for 3 to 5 days.

Quasi-static tests were conducted and different parameters for FRP laminates and front composite armors were obtained as given in Table 4.

The percentages of matrix content were in the range 15-20% for all FRP laminates and front composite armors. The areal densities of FRP-steel plates were calculated according to the following formula

$$\rho_A = \rho_c h_c + \rho_s h_s \quad (1)$$

where  $\rho_A$  is the total areal density of the FRP-steel plates,  $\rho_c$ ,  $h_c$  and  $\rho_s$ ,  $h_s$  are the mass density and thickness of front composite armor and steel backing plate, respectively.

## 2.2 Projectiles

The projectiles employed in the present tests were hemispherical nosed with a nominal mass and diameter of 25.8 g and 14.9 mm, respectively. However, the projectile mass in each test was measured in order to minimize the error in calculation of projectile kinetic energy. The materials of projectiles were quenched 45 steel, which was a type of hardened tool steel with a yield strength of 355 MPa and ultimate tensile strength in the range 450 MPa to 685 MPa in as received condition. A schematic and photograph of a projectile were shown in Fig. 1.

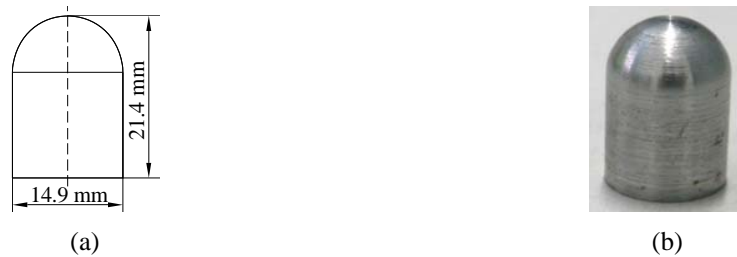


Fig. 1 (a) Schematic and (b) a photograph of projectile



Fig. 2 Photographs of test set-up: (a) clamped targets; (b) velocity measured system

### 2.3 Test set-up

A smooth-bore 15-caliber powder gun of fixed barrel was used for firing the projectiles at velocities ranged from 200 m/s to 400 m/s, which were higher than the ballistic limits of all tested targets. A 300 mm by 300 mm fully clamped square boundary condition was employed, as indicated in Fig. 2(a). Initial and residual velocities of projectiles were measured fairly accurately with the help of two sets of aluminum foil screens of thickness  $6\ \mu\text{m}$ , pasted firmly on square steel frames with a free span of 300 mm as shown in Fig. 2(b).

The foils acted as a switch and produced signals in the form of voltage transmitted to the high dynamic digital storage oscilloscope (Hitachi VC7104 with the highest frequency of 100 MHz) as soon as they were perforated. The whole penetration process was captured by a digital high-speed video camera (Photron Fastcam Ultima ADX-i2) operating at a constant framing rate of 8000 fps. A schematic of the test set-up was shown in Fig. 3.

### 3. Experimental results

Penetration processes and the flying attitudes of projectiles were photographed by a high-speed video camera. A representative was shown in Fig. 4 in time sequence for test no. 3. It can be observed that the projectile normally penetrated the target and basically kept horizontal ballistic trajectory after perforation of the target.

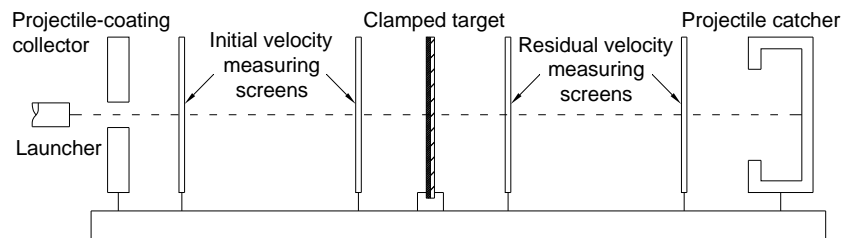


Fig. 3 A schematic of the experimental set-up

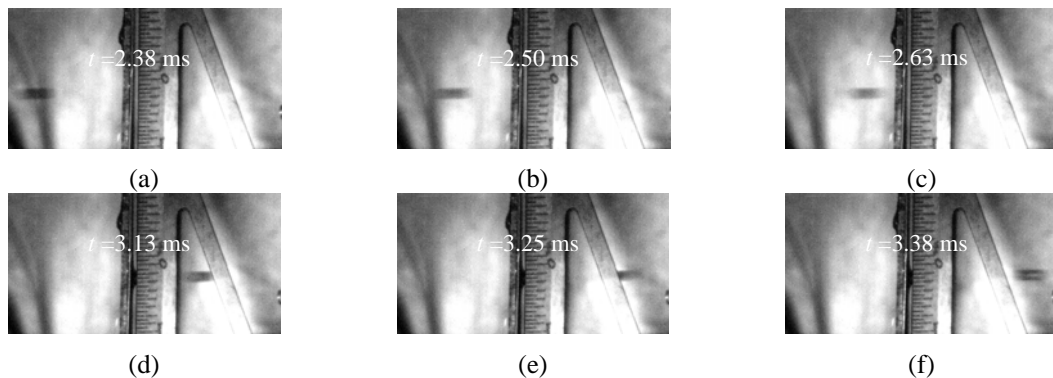


Fig. 4 Penetration process of test no. 3

No sign of large deformation of the projectiles was observed in any test and the projectiles can be regarded as rigid and nondeformable. The total energy absorbed by the target plate ( $E_t$ ) and the specific energy absorption ( $E_A$ ) or what is referred to as the energy absorption per unit areal density of target plate are respectively calculated by

$$E_t = m_p(v_i^2 - v_r^2)/2, \quad E_A = E_t / \rho_A \quad (2)$$

where  $m_p$ ,  $v_i$  and  $v_r$  are the mass, initial velocity and residual velocity of the projectile, respectively.  $\rho_A$  is the total areal density of the target plate.

Experimental results and some related parameters are presented in Table 5. In this table,  $h_c$  is the thickness of FRP laminates or front composite armors,  $h_s$  is the thickness of steel plates or steel backing plates. It should be pointed out that the weights of the epoxy resin adhesive used to bond front composite armors and steel backing plates for adhesively bonded FRP-steel plates had already been incorporated in the thickness  $h_c$ .

Table 5 Experimental results along with related main parameters

Target number	Test no.	$h_c$ (mm)	$h_s$ (mm)	$m_p$ (g)	$v_i$ (m/s)	$v_r$ (m/s)	$E_A$ (J·m <sup>2</sup> /kg)	Average $E_A$ (J·m <sup>2</sup> /kg)
1	1	—	1.36	25.7	—	316.8	—	20.4
	2	—	1.37	25.6	352.1	314.2	30.2	
	3	—	1.36	25.7	317.1	288.7	20.8	
	4	—	1.36	25.8	277.0	245.7	19.9	
	5	—	1.36	25.7	259.5	232.7	16.0	
	6	—	1.36	25.8	187.7	152.6	14.5	
2	7	1.858	—	25.8	347.4	316.0	87.7	86.5
	8	1.858	—	25.8	315.3	279.4	89.9	
	9	1.834	—	25.8	361.3	339.2	66.0	
	10	1.839	—	25.8	292.5	250.8	96.3	
	11	1.867	—	25.7	304.9	—	—	
	12	1.848	—	25.8	298.1	258.5	93.3	
3	13	1.990	1.36	25.6	333.2	—	—	31.9
	14	1.962	1.36	25.7	349.1	293.3	33.3	
	15	1.957	1.36	25.8	374.4	321.9	34.2	
	16	1.929	1.36	25.8	324.3	268.2	31.2	
	17	1.943	1.36	25.7	309.0	253.1	29.3	
4	18	0.983	1.36	25.7	344.3	292.8	34.6	32.0
	19	0.993	1.35	25.7	311.8	—	—	
	20	0.988	1.35	25.6	309.2	252.1	33.8	
	21	0.983	1.35	25.7	284.9	220.9	34.3	
	22	0.979	1.35	25.8	355.5	320.8	25.0	

Table 5 Continued

	23	2.841	1.35	25.7	359.5	301.4	32.5	
	24	2.822	1.35	25.8	295.5	216.8	34.3	
5	25	2.784	1.35	25.8	260.6	156.9	37.0	34.1
	26	2.822	1.36	25.6	210.3	—	—	
	27	2.784	1.35	25.6	325.7	256.8	34.1	
	28	1.896	1.36	25.8	360.5	—	—	
	29	1.815	1.36	25.8	317.3	267.7	27.6	
6	30	1.777	1.36	25.7	332.1	279.9	30.3	32.1
	31	1.782	1.36	25.8	318.3	258.1	33.1	
	32	1.740	1.36	25.6	378.5	322.6	37.3	
	33	1.798	1.35	25.8	221.0	167.7	18.7	
	34	1.790	1.36	25.7	311.7	—	—	
7	35	1.787	1.35	25.8	308.1	245.0	31.4	27.0
	36	1.783	1.35	25.7	276.4	220.6	25.0	
	37	1.805	1.36	25.8	354.6	298.8	32.7	
	38	2.218	1.35	25.7	332.9	273.4	33.0	
	39	2.238	1.35	25.8	343.5	284.1	34.1	
	40	2.208	1.35	25.6	295.3	224.8	33.4	
8	41	2.228	1.34	25.7	264.4	186.6	32.2	33.3
	42	2.243	1.34	25.6	—	225.7	—	
	43	2.228	1.34	25.6	295.8	226.7	33.0	
	44	2.238	1.34	25.6	326.0	263.4	33.6	
	45	2.043	1.36	25.8	369.0	308.7	38.0	
	46	2.033	1.35	25.8	—	244.8	—	
	47	2.033	1.35	25.6	266.5	—	—	
9	48	2.052	1.36	25.6	296.7	205.5	42.2	41.7
	49	2.043	1.36	25.7	256.2	135.4	43.8	
	50	2.038	1.36	25.6	309.9	223.2	42.7	

## 4. Failure mechanisms

### 4.1 Single steel plates

As far as failure mechanism were concerned, plugging and petalling were respectively the primary failure mode for thin metallic plates perforated by blunt- and conical-nosed projectiles in sub-ordnance velocity regime (Backman and Goldsmith 1978). In other words, projectiles with blunt nose tend to cause failure by plugging, while conical-nosed projectiles are prone to give petalling in thin plates (Corbett *et al.* 1996). As presented in Table 5, tests from no. 1 to no. 6 were conducted for single steel plates. Typical deformed steel plates for tests no. 4 and no. 2 were

shown in Figs. 5(a) and (b), respectively.

From Fig. 5, it can be observed that there was thinning of the target material in the contact region as well as necking occurred around the perforated hole. The diameter of the perforated hole was found to be slightly smaller than that of the projectile, due to elastic recovery. Dishing deformation took place in the remaining part of the plate near the contact region and the effect of dishing deformation was more pronounced at lower velocity.

As shown in Fig. 5, steel plates seemed to be failed by tensile stretching after severe indentation and thinning of the target material. This is due to the fact that during the penetration process, the hemispherical-nosed projectile first indents the target, causing a much localized bulge and then target thinning, which result in regions of intense tensile strain. As the deformation continues, the material in the intense tensile region starts to neck. When the tensile strain exceeds the failure strain of the target material, a spherical cap-shaped plug of reduced thickness and considerably smaller diameter than that of the projectile is removed from the target plate, with further cracking occurring in the radial direction. The plugs ejected from the target plates were collected after tests and some of them had been collected as shown in Fig. 6.



Fig. 5 Damage view of steel plates for: (a) test no. 4,  $v_i=277.0$  m/s; (b) test no. 2,  $v_i=352.1$  m/s

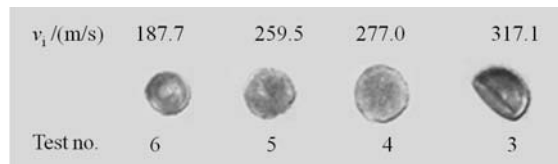


Fig. 6 Some plugs collected after tests



Fig. 7 Damage view of FRP laminate for test no. 11: (a) front view; and (b) rear view

## 4.2 FRP laminates

According to the research on perforation of high-strength fabric targets by Lim *et al.* (2002), there were mainly four types of failure mechanisms for fabric targets, namely yarn rupture, fibrillation, friction and bowing. In present experiments, the failure modes of FRP laminates are similar to those for fabric targets in Lim *et al.* (2002) since the FRP laminates are very thin and fail by the combined effects of several perforation mechanisms. The front and back views of the perforated FRP laminate for test no. 11 were shown in Figs. 7(a) and (b), respectively. From the front view (Fig. 7(a)), it can be observed that at the periphery of the contact zone, a few of fibers were sheared by the projectile. However, as shown in Fig. 7(b), most of fibers, especially on the distal side of the FRP laminate, were stretched to failure. Additionally, obscure frictional effects were observed and minimal bowing occurred on the impact side of the FRP laminate. Meanwhile, effect of fibrillation was observed on the exit side of the FRP laminate.

## 4.3 FRP-steel plates

### 4.3.1 Front composite armors

A damage view of the front composite armor in test no. 16 has shown in Fig. 8, where the front composite armor was made of CT736 fabrics and the manufacturing method was hot molding. According to Fig. 8, the failure mechanism of the front composite armor was similar to that of the FRP laminate as shown in Fig. 7. From the front view in Fig. 8, it can be observed that there are also a few of fibers sheared by the projectile around the perforation on the impact side. Nevertheless,

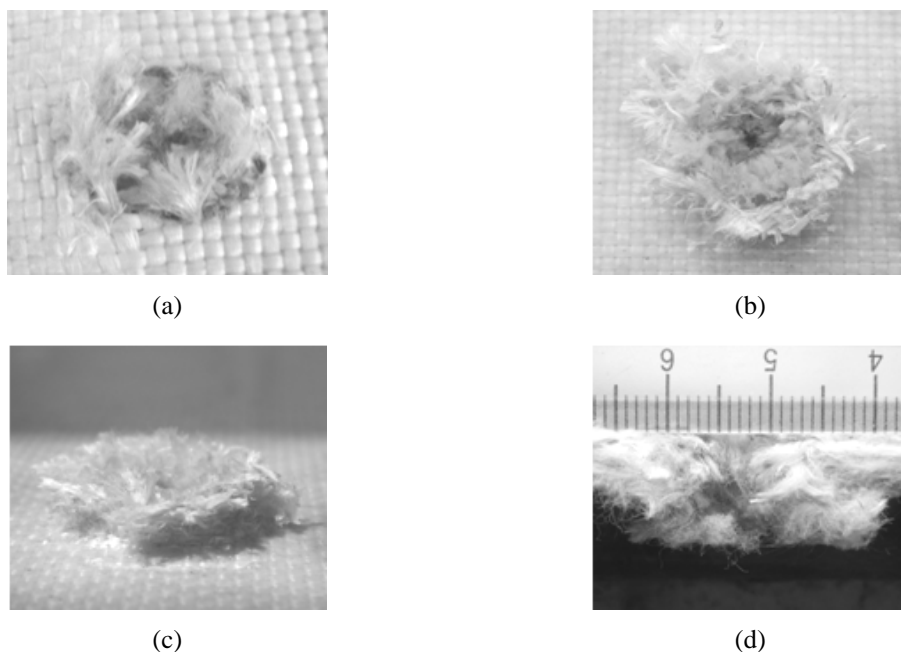


Fig. 8 Damage view of the hot-molded front composite armor made of CT736 fabrics in test no. 16. (a) Front view; (b) rear view; (c) side view; and (d) sectional view

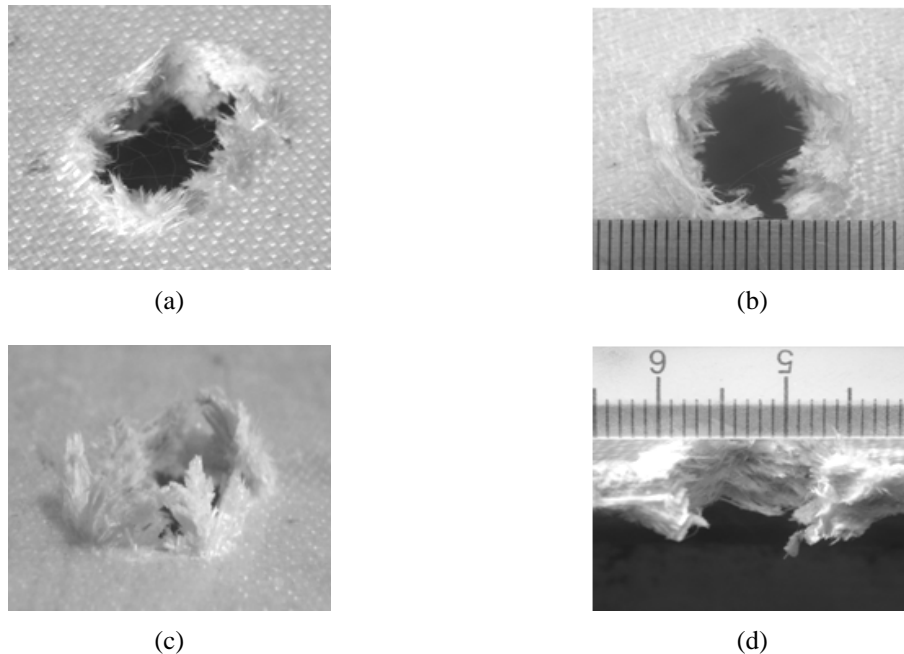


Fig. 9 Damage view of the hot-molded front composite armor made of SW220 fabrics in test no. 36: (a) front view; (b) rear view; (c) side view; and (d) sectional view

Nevertheless, the amount of the fibers sheared by the projectile in front composite armor are slightly larger than that for the FRP laminate, as expected, since the front composite armor is backed by a steel plate while the FRP laminate is not. However, it can be observed from Fig. 8 that most of the fibers were ruptured by the stretching action resulted from the moving of the projectile. This can be seen more clearly from the rear view of the Fig. 8. A certain amount of fibrillation occurred in some fibers ruptured by stretching as shown in Fig. 8(b). This is due to the fabric-fabric abrasion in the direction perpendicular to the length of the fibers (Lim *et al.* 2002). In order to directly check over the through-thickness transition of damage modes from shearing failure to stretching rupture, some front composite armors were sectioned by a water reamer in the impact region and a representative sectional view was given in Fig. 8(d). It can be obtained from Fig. 8d that the proportion of the fibers failed by shearing is very small and most of fibers through thickness are failed by stretching. From the damage view of the front composite armor observed from experimental results, it can be concluded that the failure mechanism of front composite armors is predominantly stretching rupture of fibers. Meanwhile, the damaged fibers are localized in the impact region and the size of the damage region is approximately equal to the diameter of the projectile. Failure mechanisms of the front composite armors made of T750 fabrics using hot molding method as well as the front composite armors made of CT736 fabrics using hand lay-up method are both similar to that of the front composite armors made of CT736 fabrics using hot molding method.

The failure mechanism of the front composite armors made of SW220 fabrics by hot molding is quite different from that of the front composite armor made of CT736 fabrics or T750 fabrics. Fig.

9 is the damage view of the front composite armor made of SW220 fabrics using hot molding method in test no. 36. It can be clearly observed from both of the front view and the rear view of Fig. 9 that most of the fibers in the impact region are sheared by the projectile. A very few of fibers on the distal side are failed by stretching as shown in Fig. 9(c). Further observation from Fig. 9(c) shows that the damaged fibers were essentially localized in the impact region and in the other part of the front composite armor there is no sign of visible deformations. The front composite armor in test no. 36 was also sectioned in the impact region and the sectional view was given in Fig. 9(d). It is evidently observed from Fig. 9(d) that absolute majority of fibers in the impact region are failed by shearing through thickness. Meanwhile, it can be also seen from Fig. 9(d) that the diameter of the damage region is approximately equal to that of the projectile. In comparison with the front composite armor made of CT736 fabrics (see Fig. 8(d)), the fibrillation effect in the front composite armor made of SW220 fabrics is obscure to some extent in the impact region, which results in a relatively clean perforation hole as shown in Fig. 9(d).

The disparities in failure mechanisms between front composite armors made of CT736 (or T750) fabrics and those made of SW220 fabrics are mainly due to the differences in shear modulus and toughness of the fibers. As shown in Table 4, the shear modulus of the laminates made of SW220 fabrics was generally two times that of laminates made of CT736 (or T750) fabrics. However, the toughness of the laminates made of SW220 fabrics was much lower than that of laminates made of CT736 (or T750) fabrics. For composite laminates, increasing shear modulus will lead to the increase of shear stiffness and then make the occurrence of transverse deflections in fiber layers more difficult. So, FRP laminates with relatively high shear modulus tend to be failed by shearing when impacted by projectiles. Meanwhile, the toughness of fibers also has large influence on the failure modes of FRP laminates and those made of fabrics with relatively lower toughness are prone to produce shear failure when impacted by projectiles. Therefore, front composite armors made of SW220 fabrics are predominantly failed by shearing, while those made of CT736 or T750 fabrics are mainly failed by tensile rupture of fibers.

#### 4.3.2 Steel backing plates

Due to the influences of front composite armors, failure mechanisms of steel backing plates in FRP-steel plates have greatly changed in comparison with single steel plates. Fig. 10 gives the damage views of some perforated steel backing plates. As shown in Fig. 10, petalling is the dominant failure mode for steel backing plates, although in some cases there is a plug of small size produced at the center of the impact region. Meanwhile, there are some radial cracks which form the petals in the impact region and at lower impact velocities the cracks are larger and the number of the petals is smaller but their sizes are greater. When the failure mechanism of the steel backing plate is between petalling and plugging (Fig. 10(f)) in the case of relatively higher impact velocity, the cracks are relatively small and the number of petals is larger and the petals are almost square in shape.

The differences in failure modes between single steel plates and steel backing plates are mainly attributed to two aspects. On one hand, for a FRP-steel plate penetrated by a projectile, the velocity of the projectile when impacts the steel backing plate has been greatly lowered after the perforation of front composite armor. According to the previous study by Dean *et al.* (2009) on perforation mechanism for a thin steel plate impacted by a hemispherical-nosed projectile at low velocity, the radius of bulging region in a steel backing plate which ultimately forms a cap-shaped plug reduces with decrease of impact velocity. In other words, the lower the projectile impact

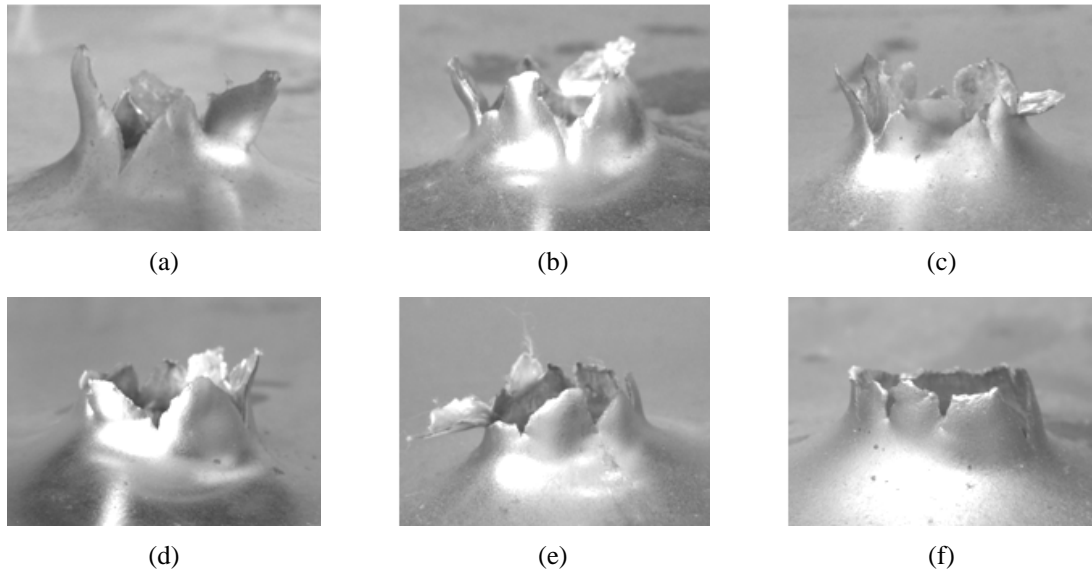


Fig. 10 Damage views of some steel backing plates in: (a) test no. 47,  $v_i = 266.5\text{m/s}$ ; (b) test no. 40,  $v_i = 295.3\text{m/s}$ ; (c) test no. 35,  $v_i = 308.1\text{m/s}$ ; (d) test no. 30,  $v_i = 332.1\text{m/s}$ ; (e) test no. 27,  $v_i = 325.7\text{m/s}$ ; (f) test no. 15,  $v_i = 374.4\text{m/s}$

velocity, the more difficult that shear plugging occurs in the steel backing plate. On the other hand, during the process of perforating steel backing plate, fractured fibers generated from front composite armor attached on the surface of projectile nose. This increases the area of impact region in steel backing plate as well as equivalently increases the diameter of the projectile in the process of extruding the initial hole. Thus, circumferential stresses at the edge of the initial hole rapidly reached the yield stress of the target material and then cracks occurred. Due to the further extrusion of the projectile whose nose was attached with fractured fibers, these cracks propagated in the radial direction and in the meantime, petals were formed and then bended until the process of petalling ended. Besides the two main reasons mentioned above, frictions between the attached fractured fibers and the surface of projectile nose also made the projectile velocity decrease. Consequently, the dominant failure mode of steel backing plates was greatly changed due to the influence of front composite armors in comparison with single steel plates.

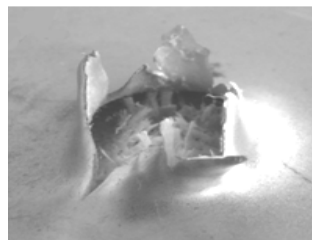


Fig. 11 Damage view of the FRP-steel plate in test no. 47

Table 6 Measured average crack length, average crevasse diameter and observed failure modes for steel backing plates

Test no.	Number of petals $n$	Average crack length $l$ /mm	Average crevasse diameter $D$ /mm	$D/d$	Failure modes
13	5	9.8	21.7	1.5	Petalling
14	7	8.3	18.2	1.2	Petalling
15	5	5.3	19.0	1.3	Petalling/plugging
16	6	7.1	17.3	1.2	Petalling
17	5	8.4	19.2	1.3	Petalling
18	4	5.8	19.5	1.3	Petalling/plugging
19	5	6.9	17.4	1.2	Petalling
20	4	9.4	19.5	1.3	Petalling
21	4	7.1	23.0	1.5	Petalling
22	3	3.7	17.4	1.2	Petalling/plugging
23	7	6.9	17.3	1.2	Petalling
24	6	7.7	18.8	1.3	Petalling
25	5	10.3	22.3	1.5	Petalling
26	5	10.8	25.5	1.7	Petalling
27	6	6.9	18.7	1.3	Petalling
28	4	5.0	17.9	1.2	Petalling/plugging
29	6	7.7	19.8	1.3	Petalling
30	6	8.5	20.7	1.4	Petalling
31	5	9.5	24.3	1.6	Petalling
32	6	7.4	17.9	1.2	Petalling
33	4	10.9	25.8	1.7	Petalling
34	4	7.1	19.8	1.3	Petalling
35	6	8.2	19.7	1.3	Petalling
36	—	—	18.9	1.3	Hinged cap
37	5	8.5	20.1	1.4	Petalling
38	6	9.0	19.1	1.3	Petalling
39	6	8.9	19.4	1.3	Petalling
40	5	8.8	19.2	1.3	Petalling
41	3	11.2	23.6	1.6	Petalling
42	4	7.3	18.6	1.2	Petalling
43	4	9.9	22.3	1.5	Petalling
44	5	8.6	18.5	1.2	Petalling
45	5	4.6	17.9	1.2	Petalling/plugging
46	5	7.9	18.4	1.2	Petalling
47	5	9.7	20.4	1.4	Petalling
48	5	8.3	18.8	1.3	Petalling
49	4	12.0	27.7	1.9	Petalling
50	6	8.1	21.1	1.4	Petalling

Further observations showed that the ultimate crevasses in steel backing plates were almost of circular shape. Table 6 listed the sizes of petalling crevasses in steel backing plates for tests from no. 13 to no. 50, where  $d$  is the projectile diameter. It can be seen that the number of petals for steel backing plates varies between four and seven with five being the most common. The average diameters of crevasses for steel backing plates are between 1.2 and 2 times the projectile diameter. This is just due to the effect of fractured fibers attached on the surface of projectile nose. A representative damage view of a FRP-steel plate in test no. 47 was shown in Fig. 11.

## 5. Impact energy absorption

### 5.1 Single steel plates

For single steel plates, the specific energy absorption increases with increasing initial projectile velocities as shown in Fig. 12. This is mainly due to the strain-rate sensitivity of the mild steel and the plugging effect (Dean *et al.* 2009). As the initial velocity of the projectiles increases, the strain rate of the mild steel increases, making the dynamic strength of the steel plate correspondingly increase. However, the plugging effect of the projectile gives much more contribution to the total energy absorption of the steel plates than strain-rate effect does. This is obviously attributed to the fact that the flying velocity of the plug after detached from target plate is at least as large as the residual velocity of the projectile and increases with the increase of the initial projectile velocity. Therefore, the total energy absorption calculated by Eq. (2) includes the kinetic energy of the cap-shaped plug in the case of perforation of a single steel plate. The specific energy absorptions of single steel plates are between  $14 \text{ J}\cdot\text{m}^2/\text{kg}$  and  $31 \text{ J}\cdot\text{m}^2/\text{kg}$  as shown in Table 5. Nevertheless, in the velocity range investigated in present tests, the contribution to the total energy absorbed due to the plug effect should be significant and the ratio of the energy absorbed due to shear plugging to the total absorbed energy increases with the initial projectile velocity.

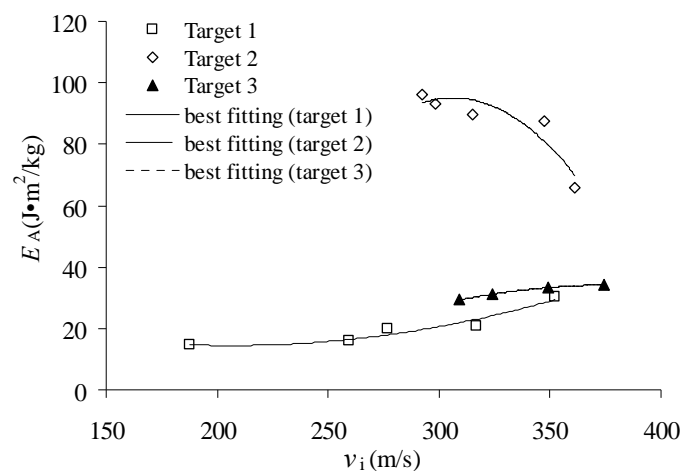


Fig. 12 Specific energy absorption vs. initial velocity for targets 1-3

## 5.2 FRP laminates

Observations in present tests showed that for FRP laminates perforated by projectiles at higher impact velocities, only small parts of the laminates are deflected and the fibers failed by stretching are largely reduced. So in the case of higher impact velocity, both the deflection and breakage of fiber due to stretching are reduced and confined to a small region of the laminates. Also, it is expected that at higher impact velocity, FRP laminates are perforated so shortly that there is few time for the impact energy to be dissipated away from the impact point to the rest part of the laminates. Therefore, as the impact velocity increases, although the strain rate of the fibers increases which appreciably enhances the energy absorption of the laminates, the total energy absorbed by the laminates decreases. The plot of specific energy absorption against impact projectile velocity for FRP laminates was shown in Fig. 12. From Fig. 12, it can be seen that the trends of specific energy absorption against impact velocity between single steel plates and FRP laminates are opposite. Though cannot be obtained from the present experimental data in lower velocity range for FRP laminates, it may be inferred that the energy absorbed by FRP laminates at lower velocity should be higher than the maximum value obtained in present tests. From the experimental results shown in Table 5, we can conclude that the specific energy absorption of FRP laminates is almost between 3 and 5 times that of single steel plates with an average value of 4.3 times in the tested velocity range.

## 5.3 FRP-steel plates

For the FRP-steel plate (target 3), the specific energy absorptions are in the range 29 to 35  $\text{J}\cdot\text{m}^2/\text{kg}$ , which are in-between single steel plates and FRP laminates as shown in Fig. 12. From the above analysis of impact energy absorptions for single steel plates and FRP laminates, it is concluded that for a FRP-steel plate, front composite armor is the main energy-absorbing component and the change of its failure mode has large influence on the total perforation resistance of the FRP-steel plate. However, the thicknesses of steel backing plates in the present tests were relatively thin and the impact velocities of the projectiles were in the low velocity range. Therefore, the failure modes of the front composite armors changed slightly.

### 5.3.1 Effect of relative thickness of front composite armors

Targets 3-5 were all adhesively-bonded FRP-steel plates, whose front composite armors were made of the same type of fabrics and prepared by the same manufacturing method. The only difference between targets 3-5 was the relative thicknesses of the front composite armors (the thickness ratio of the front composite armor to steel backing plate), which were increased successively for targets 4, 3 and 5. In this section, the average specific energy absorptions for targets 4, 3 and 5 were compared with each other. From Table 5, it can be obtained that the average specific energy absorptions for targets 4 and 3 are nearly the same in the tested velocity range, which are equal to  $31.9 \text{ J}\cdot\text{m}^2/\text{kg}$  and  $32.0 \text{ J}\cdot\text{m}^2/\text{kg}$ , respectively. This is due to the small difference in the relative thicknesses of front composite armors for targets 3 and 4, which make the effect of relative thickness on average specific energy absorption be not evident. In test 22, thin thickness of front composite armor as well as high impact velocity of projectile led to large extent of sheared fibers, which resulted in low ballistic-resistant capability of front composite armor. Meanwhile, the projectile velocity when impacted the steel backing plate was relatively high, which made the shear effect in steel backing plate be obvious. Thus, the ballistic-resistant capability of the steel backing plate was also decreased. Therefore, the total impact energy

absorption of the combined target in test 22 was relatively lower. For target 5, however, the average specific energy absorption reaches  $34.5 \text{ J}\cdot\text{m}^2/\text{kg}$ . The increase of average specific energy absorption is mainly due to the increase of relative thickness of front composite armor in target 5. Through the analysis of failure mechanisms conducted above, it was seen that an amount of sheared fibers were produced at the impact side of front composite armor. Thus, the increase of the thickness of front composite armors will lead to the increase of proportion of tensile ruptured fibers in through-thickness direction, and meanwhile, make petalling occur in steel backing plates more easily. Consequently, the whole impact-energy-absorbing capability of combined targets will be enhanced. Generally, it can be concluded that the average specific energy absorption of FRP-steel plates increases with increasing the relative thicknesses of front composite armors.

### *5.3.2 Effect of manufacturing method of front composite armors*

The effect of manufacturing method of front composite armors on the average energy absorption of FRP-steel plates was investigated as for targets 3 and 6. Those two types of FRP-steel plates were different from each other just because of the different manufacturing methods of their front composite armors as listed in Table 3. It was obtained that the average specific energy absorptions for targets 3 and 6 are equal to  $32.0 \text{ J}\cdot\text{m}^2/\text{kg}$  and  $32.1 \text{ J}\cdot\text{m}^2/\text{kg}$ , respectively and minor difference was gained in terms of the average specific energy absorptions between target 3 and target 6. This is mainly attributed to the presence of steel backing plates, which makes delamination difficult to occur in front composite armors. Moreover, because the front composite armors are relatively thin, the energy absorbed due to delamination is so small that it can be completely neglected. More importantly, tensile rupture of fibers is the dominant failure mode for the front composite armor and most of the energy is absorbed by this failure mode. Although the relative thickness of front composite armor as well as the initial projectile velocity have some influences on the total energy absorption of a FRP-steel plate, it is reasonable to conclude that in sub-ordnance velocity regime, manufacturing methods of front composite armors, i.e., hot-molding and hand lay-up, have little effects on the total perforation resistance of FRP-steel plates.

### *5.3.3 Effect of fabric type of front composite armors*

For investigation of the effect of fabric types of the front composite armors on the total perforation resistance of FRP-steel plates, three types of fabrics are considered as shown in Table 3, namely CT736 fabric in targets 3, T750 fabric in target 7 and SW220 fabric in target 8. The average specific energy absorptions for target 3, target 7 and target 8 are equal to  $32.0 \text{ J}\cdot\text{m}^2/\text{kg}$ ,  $26.9 \text{ J}\cdot\text{m}^2/\text{kg}$  and  $33.2 \text{ J}\cdot\text{m}^2/\text{kg}$ , respectively. Comparison of average specific energy absorptions between targets 3, 7 and 8 showed that the average specific energy absorption of target 8 is a little larger than that of target 3. This is mainly attributed to the relatively lower initial projectile velocities for target 8. However, the average specific energy absorption for target 7, whose front composite armor is made of SW220 fabrics, is about 15.8% less than that of target 3 and 18.9% less than that of target 8. This is mainly due to the relatively smaller ultimate tensile strength for SW220 fiber compared with CT736 and T750 fibers as shown in Table 4. In addition, glass fiber is a type of brittle fibers and its toughness is greatly smaller than that of aramid fiber, which makes shearing failure occur more easily in SW220 fabric compared with CT736 or T750 fabrics in perforation process. The fact that the energy per unit volume absorbed due to shearing failure of fibers is much smaller than that due to tensile failure of fibers leads to relatively lower energy-absorbing capability for the FRP-steel plates whose front composite armor is made of

SW220 fabrics.

#### 5.3.4 Effect of joining type of FRP-steel plates

Effect of joining styles between front composite armor and steel backing plate on the specific energy absorption of FRP-steel plates was investigated for targets 8 and 9, in which the steel backing plates were adhesively bonded and not adhesively bonded (in-contact) to the rear faces of front composite armors, respectively. From Table 5, it is obtained that the average specific energy absorptions for target 8 and target 9 are  $33.2 \text{ J}\cdot\text{m}^2/\text{kg}$  and  $41.7 \text{ J}\cdot\text{m}^2/\text{kg}$ , respectively. Comparison of the effect of joining styles on average specific energy absorptions of FRP-steel plates (target 8 and target 9) were performed. It can be obtained that the average specific energy absorption of the in-contact FRP-steel plate (target 9) is about 25.5% higher than that of the adhesively-bonded FRP-steel plate (target 8). This is mainly due to the adhesion between the front composite armor and the steel backing plate, which makes the deformation as well as the tensile rupture of fibers be difficult to occur in front composite armor because of the restriction resulted from steel backing plate during the perforation process. Thus, compared with FRP laminates, the energy absorbed due to stretching failure of fibers in the contact region as well as the deformation energy in the other region for front composite armors are greatly reduced, which, consequently, make the total energy absorbed by adhesively-bonded FRP-steel plates be less than that by in-contact FRP-steel plates. Therefore, it can be concluded that for a FRP-steel plate, the higher adhesive strength between the front composite armor and the steel backing plate, the lower the perforation resistance of the FRP-steel plate.

## 6. Conclusions

The ballistic performance of the FRP-steel plates was experimentally researched and the comparisons between FRP-steel plates, FRP laminates and steel plates were made. The main conclusions in the present article are:

- Under ballistic impact by hemispherical-nosed projectiles in the sub-ordnance velocity regime, the energy absorbing capability of FRP laminates is much higher than that of steel plates. Thus, in a FRP-steel plate, front composite armor is the main energy-absorbing component and the change of its failure modes has significant influence on the total perforation resistance of the FRP-steel plate.
- For a FRP-steel plate under low velocity impact, steel backing plate has slight influence on the failure mode of the front composite armor. However, front composite armor has a significant influence on the failure mechanism of steel backing plate, which improves the energy-absorbing capability of steel backing plate. Due to the influence of front composite armor, the dominate failure mode of steel backing plate has been greatly changed.
- The relative thickness and fabric type of the front composite armor have relatively large influences, whereas the manufacturing method of the front composite armor, i.e., hot-molding and hand lay-up, has slight influence on the total perforation resistance of a FRP-steel plate. Moreover, joining style between the front composite armor and steel backing plate in a FRP-steel plate also has considerable effect on its total perforation resistance in the case of FRP-steel plates perforated by hemispherical-nosed projectiles in the sub-ordnance velocity regime.

## Acknowledgments

This work is financially supported by the National Natural Science Foundation of China (under Grant Nos. 51179200, 51209211), and the Innovation Research Foundation for Ph. D Candidates of Naval University of Engineering, P. R. China (under Grant No. HGYJSJJ2012001), which are all gratefully acknowledged.

## References

- Almohandes, A.A., Abdel-Kader, M.S. and Eleiche, A.M. (1996), "Experimental investigation of the ballistic resistance of steel-fiberglass reinforced polyester laminated plates", *Compos. Part B: Eng.*, **27**(5), 447-458.
- Backman, M.E. and Goldsmith, W. (1978), "The mechanics of penetration of projectiles into targets", *Int. J. Eng. Sci.*, **16**(1), 1-99.
- Ben-Dor, G., Dubinsky, A. and Elperin, T. (1998a), "On the ballistic resistance of multi-layered targets with air gaps", *Int. J. Solids Struct.*, **35**(23), 3097-3103.
- Ben-Dor, G., Dubinsky, A. and Elperin, T. (1998b), "Effect of air gaps on ballistic resistance of targets for conical impactors", *Theoret. Appl. Fract. Mech.*, **30**(3), 243-249.
- Ben-Dor, G., Dubinsky, A. and Elperin, T. (2006), "Effect of air gaps on the ballistic resistance of ductile shields perforated by non-conical impactors", *J. Mech. Mater. Struct.*, **1**(2), 279-299.
- Chen, C.H., Zhu, X., Hou, H.L. and Wang, T.Q. (2011), "Experimental study on composite armor structure of warship topside against kinetic armor-piercing", *Explosion and Shock Waves*, **31**(1), 11-18. [In Chinese]
- Corbett, G.G., Reid, S.R. and Johnson, W. (1996), "Impact loading of plates and shells by free-flying projectiles-a review", *Int. J. Impact Eng.*, **18**(2), 141-230.
- Corran, R.S.J., Shadbolt, P.J. and Ruiz, C. (1983), "Impact loading of plates-an experimental investigation", *Int. J. Impact Eng.*, **1**(1), 3-22.
- Dean, J., Dunleavy, C.S., Brown, P.M. and Clyne, T.W. (2009), "Energy absorption during projectile perforation of thin steel plates and the kinetic energy of ejected fragments", *Int. J. Impact Eng.*, **36**(10-11), 1250-1258.
- Dey, S., Borvik, T., Teng, X., Wierzbicki, T. and Hopperstad, O.S. (2007), "On the ballistic resistance of double-layered steel plates-an experimental and numerical investigation", *Int. J. Solids Struct.*, **44**(20), 6701-6723.
- Elek, P., Jaramaz, S. and Mickovic, D. (2005), "Modeling of perforation of plates and multi-layered metallic targets", *Int. J. Solids Struct.*, **42**(3-4), 1209-1224.
- Gupta, N.K. and Madhu, V. (1997), "An experimental study of normal and oblique impact of hard-core projectile on single and layered plates", *Int. J. Impact Eng.*, **19**(5-6), 395-414.
- Gupta, N.K., Iqbal, M.A. and Sekhon, G.S. (2008), "Effect of projectile nose shape, impact velocity and target thickness on the deformation behavior of layered plates", *Int. J. Impact Eng.*, **35**(1), 37-60.
- Kreyenhagen, K.N., Wagner, M.H., Piechocki, J.J. and Wagner, M.H. (1970), "Ballistic limit determination in impacts on multimaterial laminated targets", *AIAA J.*, **18**(12), 2147-2151.
- Liang, C.C., Yang, M.F., Wu, P.W. and Teng, T.L. (2005), "Resistant performance of perforation of multi-layered targets using an estimation procedure with marine application", *Ocean Eng.*, **32**(3-4), 441-468.
- Lim, C.T., Tan, V.B.C. and Cheong, C.H. (2002), "Perforation of high-strength double-ply fabric system by varying shaped projectiles", *Int. J. Impact Eng.*, **27**(6), 577-591.
- Marom, I. and Bodner, S.R. (1979), "Projectile perforation of multi-layered beams", *Int. J. Mech. Sci.*, **21**(8), 489-504.
- Nia, A.A. and Hoseini, G.R. (2011), "Experimental study of perforation of multi-layered targets by

- hemispherical-nosed projectiles”, *Mater. Des.*, **32**(2), 1057-1065.
- Nurick, G.N. and Walters, C.E. (1990), “The ballistic penetration of multiple thin plates separated by an air gap”, *Proceedings of SEM Conference on Experimental Mechanics*, pp. 631-637.
- Radin, J. and Goldsmith, W. (1988), “Normal projectile penetration and perforation of layered targets”, *Int. J. Impact Eng.*, **7**(2), 229-259.
- Teng, X., Dey, S., Borvik, T. and Wierzbicki, T. (2007), “Protection performance of double layered metal shields against projectile impact”, *J. Mech. Mater. Solids*, **2**(7), 1307-1328.
- Teng, X., Wierzbicki, T. and Huang, M. (2008), “Ballistic resistance of double-layered armor plates”, *Int. J. Impact Eng.*, **35**(8), 870-884.
- Woodward, R.L. and Cimpoeru, S.J. (1998), “A study of the perforation of aluminium laminate targets”, *Int. J. Impact Eng.*, **21**(3), 117-131.
- Zhu, X., Hou, H.L., Gu, M.B., Mei, Z.Y. and Chen, X. (2006), “Experimental study on armor protection against ballistic impact of small caliber artillery”, *Explosion and Shock Waves*, **26**(3), 262-268. [In Chinese]
- Zhu, X., Mei, Z.Y. and Liu, R.Q. (2003), “Warship’s light composite armor structure resistibility for ballistic impact”, *Explosion and Shock Waves*, **23**(1), 61-66. [In Chinese]
- Zukas, J.A. and Scheffler, D.R. (2001), “Impact effects in multilayered plates”, *Int. J. Solids Struct.*, **38**(19), 3321-3328.